Microporous and Mesoporous Materials 360 (2023) 112725

Contents lists available at ScienceDirect

Microporous and Mesoporous Materials

journal homepage: www.elsevier.com/locate/micromeso

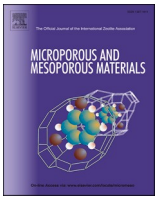

Impact of topology framework of microporous solids on methanol carbonylation: An *operando* DRIFTS-MS study

L.A. Luque-Álvarez [*], M. Serrano-Cruz, M. González-Castaño [**], L.F. Bobadilla, J.A. Odriozola

Departamento de Química Inorgánica e Instituto de Ciencia de Materiales de Sevilla, Centro Mixto CSIC—Universidad de Sevilla, Av. Américo Vespucio 49, 41092, Sevilla, Spain

ARTICLE INFO

Keywords:
Methanol carbonylation
Heterogeneous catalysts
Zeolites topology
Operando DRIFTS-MS

ABSTRACT

Methanol carbonylation was evaluated over heterogeneous catalysts based on Cu-exchanged zeolitic materials with different topology: Cu@MOR, Cu@FER, and Cu@ZSM-5. Despite the similar Si/Al ratios, it is crucial to acknowledge that the acid strength is influenced by the framework topology, as supported by the NH_3-TPD results. This, along with other characterization techniques allowed us to estimate the impact of pore size and pore distribution in these microporous materials on catalytic performance. The channel structure influenced catalytic parameters such as conversion and selectivity. The higher methanol conversion achieved on Cu@FER shows the importance of Brønsted acid sites and redox centres location regarding the topology of the material. Concerning the selectivity, the production of acetic acid was endorsed by the 12-MR (MOR) channels, methyl acetate's production by the 10-MR (FER) channels. Finally, the presence of 6-MR (ZSM-5) channels led to a complete selectivity towards DME production. The reaction mechanism was elucidated via *operando* DRIFTS-MS and results revealed a bifunctional mechanism in which methanol adsorbs and dehydrates on acidic Brønsted sites and CO is activated over Cu^+ species.

1. Introduction

Acetic acid is a key building block that is used in various industrial sectors such as food, textile or pharma [1]. Currently, more than 85% of the acetic acid produced worldwide is obtained by methanol carbonylation using the homogeneous Monsanto and Cativa™ processes, in which organometallic catalysts based on noble metals such as rhodium and iridium are used [2,3]. Despite the existence of other processes, methanol carbonylation reaction ($CH_3OH + CO \rightarrow CH_3COOH$) in liquid phase is the most widely accepted route due to the high yield obtained, the high purity of the products formed and the production of few by-products. The Monsanto process employs a Rh-based catalyst and achieves a 99% selectivity operating between 150 and 200 °C and 30 bar [4] whereas in BP Cativa™ process (in industry since 1996), by using an Ir-based catalyst in a softer conditions, the number of by-products decreases and the purity of the final product increases. Nevertheless, the cost of both catalysts, the use of iodomethane as promoter and the challenging separation and recovery of the homogeneous catalyst are relevant drawbacks which need to be surpassed.

Consequently, the heterogenization of the process using zeolite-based solid catalysts is proposed [5,6]. These microporous materials, apart from being more cost-effective, present advantages such as high surface area and thermal stability. Moreover, from a catalytic point of view, acidity can be tuned, and other properties can be improved since it is possible to provide them with a bifunctional mechanism through the incorporation of redox centres. In this sense, early studies reported by Fujimoto et al. [7] proposed the employment of Cu-exchanged mordenite-type zeolites [5,8]. The use of this metal lies in its good redox properties and that is indeed considered the most active and selective metal for carbonylation processes, even though opposing discussions have been raised on the performance of Cu metal promoted carbonylation, suggesting promoted activation of CO species and stabilization of DME [5].

For carbonylation reactions, the channel structure (see Fig. 1) has received considerable attention since it determines the reactants conversion and overall process selectivity. Methanol carbonylation reaction is demonstrated to take place in the 8-MR (Membered Rings) because of the particular orientation of the methoxy group [6]. On the other hand, larger cavities promote the generation of longer hydrocarbon and coke deposits especially at high temperatures [9,10]. The adequate spatial

* Corresponding author.
** Corresponding author.
E-mail addresses: llalvarez@us.es (L.A. Luque-Álvarez), mgonzalez6@us.es (M. González-Castaño).

https://doi.org/10.1016/j.micromeso.2023.112725
Received 15 March 2023; Received in revised form 15 June 2023; Accepted 9 July 2023
Available online 11 July 2023

constrains of 8-MR channels let the stabilization of specific reaction intermediates through the interaction with nearby oxygen atoms closer within narrower channels. Such confinement effects promote the insertion of CO into methyl groups with the corresponding formation of carbon-carbon bonds and indorse the overall carboxylation rates. Among the evaluated zeolites, mordenite (MOR) is the most active and selective followed by ferrierite (FER), both systems containing 8-MR channels. Still, the 10-MR contained within the FER systems have been associated to enhanced stabilities against carbon deposits [10].

In this context, this work evaluates the catalytic performance of Cu@MOR, Cu@FER and Cu@ZSM-5. The influence of the zeolite topology in methanol carbonylation reaction and the mechanism of the reaction itself was assessed via an *operando* DRIFTS-MS study. MOR and FER were selected due to their promising performance for the carbonylation reaction whilst ZSM-5 was considered due to its versatility in industrial applications. In this way, the role of 6-MR cavities could also be tested in the reaction. Remarkably, the comparable Si/Al ratios characterizing the chosen zeolites permitted extrapolating meaningful knowledge concerning the impact of the channels size on the methanol carbonylation reaction pathway. The obtained results highlight the importance of bifunctional Cu-exchanged zeolitic catalysts for methanol carbonylation processes, allowing to obtain acetic acid under softer conditions than conventional industrial processes.

2. Experimental

2.1. Catalysts synthesis

For this study, commercial MOR (CBV21A), FER (CP914C) and ZSM-5 (CBV2314) zeolites provided by Zeolyst International were used. The as-received commercial samples were calcined during 3 h at 600 °C using a heating rate of 2 °C/min. In this sense, the commercial zeolites (MOR, FER and ZSM-5), originally in their ammonic form, were converted to their corresponding protonic ones, referred as H-MOR, H-FER, and H-ZSM-5, respectively. The cationic exchange was conducted using a 0.01 M solution of $Cu(CO_2CH_3)_2{\cdot}H_2O$ under stirring during 24 h for H-MOR and H-ZSM-5 and 48 h for H-FER. Then, the solids were washed with distilled water, filtered, and dried at 100 °C overnight. The obtained solids were calcined during 3 h at 600 °C using a heating rate of 2 °C/min. The prepared catalysts were labelled as Cu@MOR, Cu@FER and Cu@ZSM-5.

2.2. Characterization techniques

The chemical composition of the samples was characterized by X-Ray Fluorescence (XRF) in a Zetium Minerals device. The Cu content was also analysed by Inductively Coupled Plasma Atomic Emission Spectrometry (ICP-OES) in an iCAP 7200 ICP-OES Duo (ThermoFisher Scientific) spectrometer digesting the samples in a Microwave Digestion System ETHOS EASY (Milestone). For the XRD analysis the equipment used was a PANalitycal X'Pert Pro diffractometer containing a Cu anode (Cu-Kα 40 mA, 45 kV). The diffractograms were taken with a step width of 0.05° and an acquisition time of 300 s in a 2θ range of 10–60°. SEM micrographs were obtained in a Hitachi S-4800 SEM-FEG (Scanning Electron Microscope-Field Emission Gun) equipped with an EDX analyser. The textural properties of the samples were evaluated by N_2 physisorption in a Micromeritics Triflex equipment at 77 K. Prior the physisorption measurements, the samples were degassed at 250 °C during 4 h. The specific surface area, pore volume and diameter were estimated from method Brunauer, Emmer and Teller (BET). Temperature programmed desorption of ammonia (NH_3-TPD) measurements were performed in a quartz reactor (internal diameter of 9 mm) supported on a homemade system. About 50 mg of each sample were firstly pre-treated at 250 °C for 30 min under flow of 25 mL min^{-1} of He to remove moisture. Then the samples were cooled down to 120 °C and saturated with 25 mL min^{-1} of 5% NH_3 diluted in helium for 1 h. Finally, the physically adsorbed ammonia was removed by purging with 25 mL min^{-1} of helium for 1 h and after that the desorption was carried out in a temperature range of 120–700 °C at a linear heating rate of 5 °C/min. The gas effluents were analysed on line by mass spectrometry (Pfeiffer Vacuum PRISMA PLUS) and controlled by Quadera® software. The MS ammonia signal was recorded as a function of time and temperature.

Operando DRIFTS (Diffuse Reflectance Infrared Fourier Transform Spectroscopy) experiments were carried out in a FTIR Thermo Nicolet iS50 equipment with a MCT detector coupled with a PFEIFFER Vacuum Prisma Plus mass spectrometer. The spectra were registered using ca. 40 mg of sample with a resolution of 4 cm^{-1} and 64 scans per spectrum.

2.3. Catalytic activity

The catalytic performance was evaluated in a Hastelloy 9 mm-diameter tubular reactor coupled to a microactivity PID Eng&Tech device. Thus, ca. 80 mg (100–200 μm) were loaded in the reactor and pre-activated at 400 °C under 5 vol% O_2/He during 1 h. Then, the catalytic activity was recorded at P = 8 bar with a CO/MeOH molar ratio of 5 and a temperature of 280 °C. The inlet and outlet gas mixtures composition were analysed with an Agilent 6890 N gas chromatograph equipped with an Agilent J&W DB-FATWAX Ultra Inert column.

3. Results and discussion

3.1. Structural and morphological properties

The chemical composition of the prepared samples was evaluated via XRF and ICP analysis (Table S1). The comparable Si/Al ratios (*ca.* 11 ± 0.6) showed by all zeolites contrasted with the meaningful variations attained for the Cu contents. In fact, significantly lower Cu contents were obtained for the Cu@FER (0.57 *wt*% Cu) compared to Cu@MOR and Cu@ZSM-5 (2.91 and 2.96 *wt*% Cu, respectively). The lower cation exchange capacity (CEC) observed for FER zeolite may be attributed to less accessible exchange sites, which may be due to pH or channel distribution in the solid [25]. Moreover, XRD data (Fig. S1) of the zeolitic materials in their protonic form and after the Cu incorporation evidenced no important structural variations on the zeolites. The absence of diffraction associated to Cu phases underlines the absence of Cu crystals with sizes above *ca.* 4 nm. In agreement, SEM pictures (Fig. S2) showed comparable morphological characteristics for the protonic zeolites and their parent Cu exchanged systems. Moreover, MOR and FER based systems were constituted by similar irregular and elongated particles [11,12] while ZSM-5 based ones exhibited a different morphology constituted by cubic particles with a rough surface and smoother corners [13]

Fig. 2 shows the N_2-physisorption hysteresis obtained for the H-MOR, H-FER and H-ZSM-5 with their corresponding Cu-exchanged samples. All systems exhibited type I isotherms according to the IUPAC classification characteristic of microporous solids with a narrow pore distribution [14]. In the case of FER systems, a hysteresis type H4 characteristic of aggregated particles constituting pores with uniform shape and size in which the adsorption of a monolayer takes place [15]. Table 1 lists the specific surface areas and pore structure obtained from BET analysis for the different protonic and Cu-containing zeolites. The high specific surface areas and pore size about 2–3 nm characteristic of zeolite systems were obtained for all samples. Besides, no general trends derived from the Cu exchange process regarding the surface and pore values were extrapolated since higher, similar, and lower values were noticed after the Cu-exchange step compared to their parent protonic samples.

3.2. Acidic properties

Temperature-programmed desorption of ammonia (NH_3-TPD) is one of the most typical characterization techniques for analyzing the surface

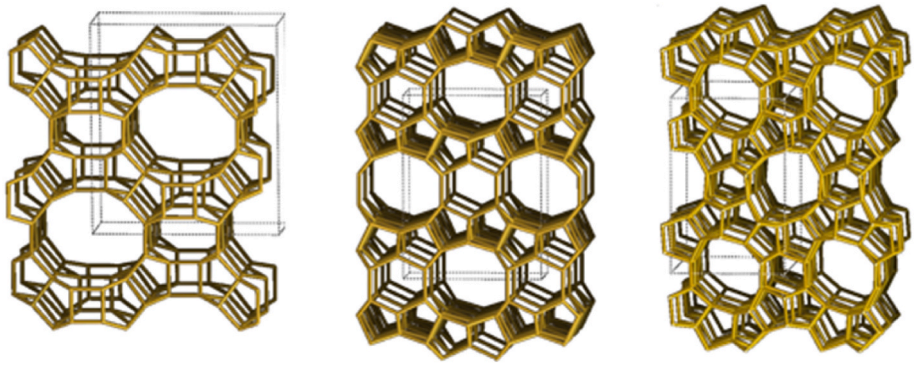

Fig. 1. From left to right, framework of mordenite (MOR), ferrierite (FER) and ZSM-5 zeolites.

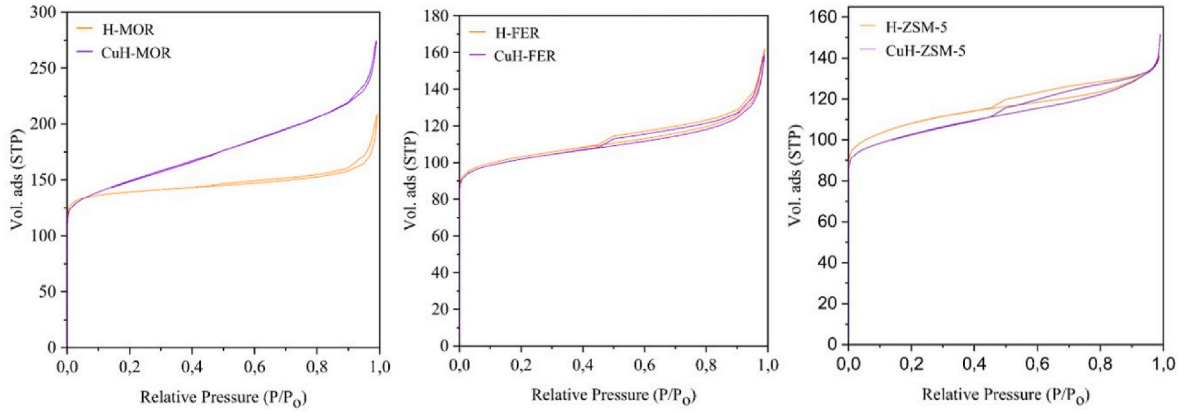

Fig. 2. Adsorption-desorption hysteresis exhibited by H- and Cu-containing zeolites.

Table 1
Textural properties of the zeolite catalysts estimated from N_2 physisorption.

	S_{BET} (m^2/g)	V_{pore} (cm^3/g)	D_{pore} (nm)
H-MOR	429	0.26	2.4
Cu@MOR	478	0.36	3.0
H-FER	317	0.21	2.6
Cu@FER	317	0.21	2.6
H-ZSM-5	340	0.12	2.4
Cu@ZSM-5	316	0.21	2.6

acidity in solid catalyst. The temperature at which ammonia is desorbed provides information about the acid strength distribution whereas the total amount of ammonia desorbed is proportional to the concentration of acidic sites.

Fig. 3A shows the NH_3-TPD profiles of the three zeolites in protonic form (H-FER, H-MOR and H-ZSM-5). As can be noticed, they are mainly composed by two peaks representing weak/moderate and strong acid sites, respectively. According to literature, the peak at low temperature can be related to weak Lewis acidic or extraframework aluminium sites while the peak at the highest temperature is attributed to strong Si–OH–Al Brønsted acid sites [16,17]. Zeolite acidity is commonly controlled by the Si/Al ratio, but in our instance, the zeolites possess analogous Si/Al ratios. Therefore, the predominance of these peaks is primarily influenced by the specific nature and topological features of the zeolite.

On the other side, Fig. 3B includes the NH_3-TPD results of the Cu-exchanged zeolites. If we compare these profiles with those obtained for the protonic form, one can see that the acidic properties are altered by the presence of copper and the distribution of weak/strong acid sites is modified. As can be observed, the addition of copper decreases the intensity of the higher temperature peak ascribed to strong Brønsted acid sites, indicating that copper was successfully exchanged in these acidic sites [18].

Specially in Cu@MOR and Cu@ZSM-5 zeolites, which exhibit a higher copper loading, it is evident that the decrease in peak intensity at elevated temperatures is accompanied by the increase in the complexity of the peaks [19,20].

In this context, the assignment of these peaks is not a straightforward task, as the inherent topology of the solid plays a crucial role in determining the specific type of acidic centres formed. Notably, the presence of distinct confinement environments primarily influences the characteristics of these centres. Within the zeolite structures, the existence of two types of confinement framework gives rise to two distinct types of Brønsted acid centres. This differentiation becomes crucial as it results in the desorption of NH_3 occurring at different temperatures [18,21]. As a result, these additional peaks can be attributed to the formation of Cu-amine complexes ionically bounded to the zeolitic framework in the different cavities of the solid [22]. Meanwhile, this fact is not such evident in the Cu@FER likely due to the lower amount of copper exchanged.

3.3. Catalytic activity

Fig. 4 shows the catalytic activity exhibited by the samples for methanol carbonylation as a function of the time on stream. Among the zeolite catalysts, significantly higher methanol conversion values were reached by Cu@FER compared to the Cu@MOR and Cu@ZSM-5 for which comparable conversions (*ca.* 60%) were determined. The highest conversion values shown by Cu@FER could be related to the concentration of Brønsted acid sites inside the cavities since these are crutial players for the generation of dimethyl ether and water via methanol dehydration [23]. Therefore, the larger concentration of Brønsted sites

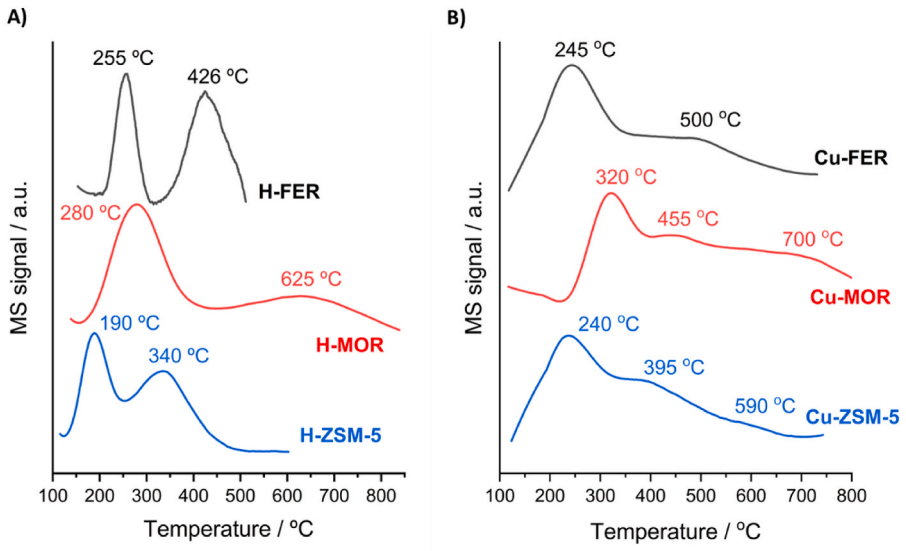

Fig. 3. A) Protonic zeolites and B) Cu-exchanged zeolites NH_3-TPD.

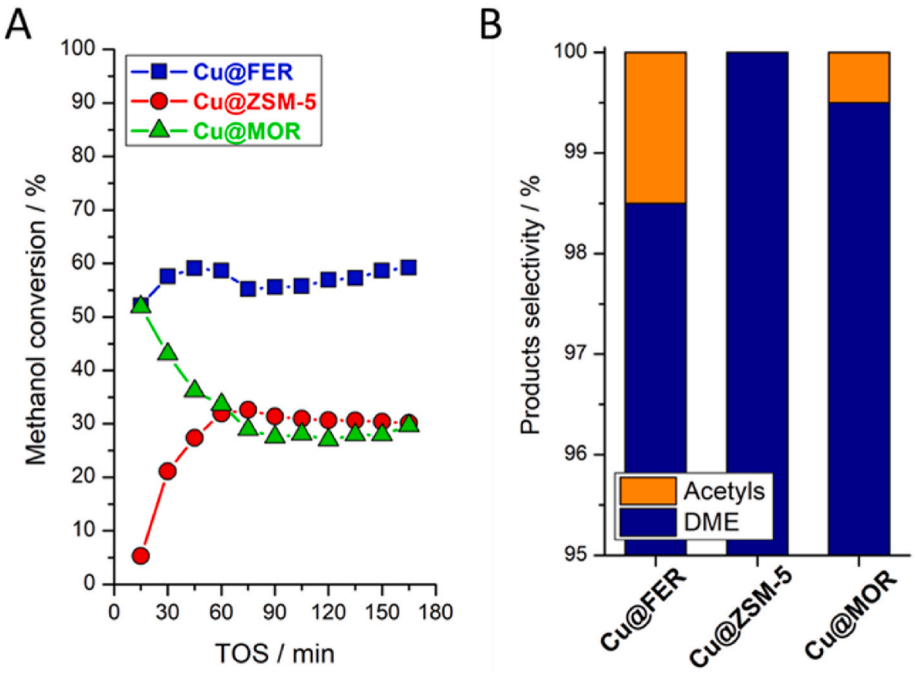

Fig. 4. Catalytic activity of the zeolite materials: A) % Methanol conversion; B) % Product selectivity.

available for the adsorption and dehydration of methanol enables higher conversion rates.

Regarding the selectivity to products (Fig. 4B), the obtained results demonstrated zeolites as highly selective systems towards the dimethyl ether formation. It can be also noticed that both Cu@FER and Cu@MOR are selective towards the formation of acetylates, i.e., methyl acetate and acetic acid. Fig. 5 displays the selectivity towards acetic acid and methyl acetate with respect time. The null production of acetic acid and the total selectivity towards the dimethyl ether production attained by Cu@ ZSM-5 might be associated to the lack of 8-MR channels, described as optimal channels for the generation and subsequent hydrolysis of methyl acetate to produce acetic acid via carbonylation processes [24]. The selectivity to acetic acid and methyl acetate attained by Cu@FER and Cu@MOR must relays on the intrinsic zeolite topology. Thus, the presence of 12-MR (MOR) and 10-MR (FER) channels affect the generation of acetyls and account for the preferential production of acetic acid and methyl acetate described by Cu@MOR and Cu@FER, respectively [25].

3.4. *Operando* DRIFTS-MS: Mechanistic study for the methanol carbonylation

Operando DRIFTS-MS spectroscopy was conducted in order to elucidate the reaction intermediates active for the methanol carbonylation, so the reaction pathway established over the surface of the different zeolites is understood. Fig. 6 shows the temporal evolution of the spectra exhibited by the different zeolites during the methanol carbonylation reaction at 200 °C and 1 bar.

In the hydroxyl region of the spectra (3800-3500 cm^{-1}), Cu@MOR sample exhibited, at 3740 cm^{-1}, the OH stretching band of silanol

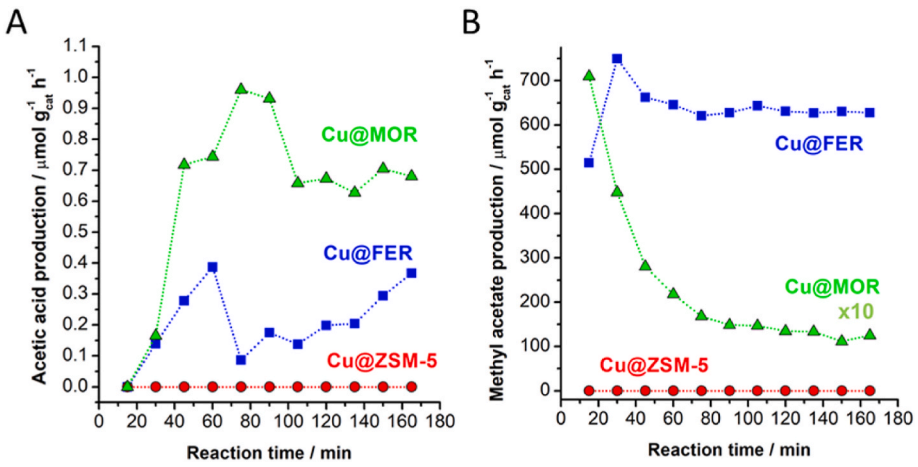

Fig. 5. A) Acetic acid and B) methyl acetate production by using zeolitic materials.

groups (Si–OH) located on the zeolite surface [26]. The OH stretching vibration associated to surface Al species (Al–OH) was observed at 3651 cm^{-1}. The acid character of Cu@MOR was evidenced from the bands observed at 3601 and 3580 cm^{-1}, being ascribed to stretching vibrations of OH bridges type Si–OH–Al placed inside the main 12-MR cavities and lateral 8-MR pockets, correspondingly [26]. With respect to Cu@MOR sample, comparable hydroxyl spectra were discerned for the Cu@FER sample for which the Si–OH stretching band appeared at 3720 cm^{-1} thereby underlining slightly higher acid strengths [27]. For Cu@ZSM-5, a single bridge Cu–OH–Al band located at 3603 cm^{-1} was identified and associated to OH species inside the 10-MR cavities.

In the C–H region (3100-2800 cm^{-1}), analogous spectra were displayed by all systems. In the case of the Cu@MOR, bands showed at 2954 and 2850 cm^{-1} were assigned to methoxy and dimethyl ether species constituted via methanol dehydration reactions at Brønsted acid sites. In this region, a weak band placed at 2963 cm^{-1} corresponding to the symmetric stretching of C–H of methyl groups corroborated the constitution of methoxy species [10]. As the methoxy and DME related bands increased, a simultaneous intensity decreases for bands placed at 3651 cm^{-1} (Al–OH), 3601 and 3580 cm^{-1} (OH species within the main cavities and side pockets, respectively) was noticed. This trend remarks that the dehydration of methanol towards DME, methoxy and water takes place over the Brønsted acid sites located inside the cavities and suggest that external Al–OH are also active players. For the Cu@MOR and Cu@FER, bands observed at 1577, 1490 and 1332 cm^{-1} might be related to acetate species. On the other hand, the generation of acetic acid most likely occurs though the hydrolysis of methyl acetate, based on the band observed 3280 cm^{-1} which can be associated to a carboxylic acid. The total selectivity to DME exhibited by the Cu@ZSM-5 sample agrees with the absence of acetate species on the catalyst surface under reaction conditions.

In the CO stretching region (2200-2000 cm^{-1}), all samples initially exhibited bands associated to carbonyl species CO–Cu^+ at 2156 cm^{-1} [28]. The comparatively low intensities observed for the carbonyl bands for Cu@FER derives from the significantly low Cu loading attained for this sample. As the reaction proceeds, another band located at 2132 cm^{-1} appears, which could be associated to CO–Cu-DME species associated to methyl acetate reaction intermediates constituted via the CO insertion [29]. The concomitant rise of the CO–Cu-DME (2132 cm^{-1}) and DME (2850 cm^{-1}) bands suggest that Cu plays a fundamental role in the methanol carbonylation reaction [9]. Moreover, the temporal evolution of the bands associated to selected reactants, surface intermediates and gas phase products is presented in Fig. 7.

For the three samples, the formation of DME (m/z = 45) at the beginning of the reaction correlates with the methanol consumption (m/z = 31). Simultaneously, the intensity bands associated to the Al–OH stretching (3651 cm^{-1}) and Si–OH–Al inside 12-MR cavities (3601 cm^{-1}) also decrease. The parallel evolution of these bands agrees with the importance of Brønsted acid sites located inside 12-MR cavities towards the generation of DME often proposed in literature [10]. It also suggests that Al–OH sites might play a significant role for the DME formation. In concordance with the IR-band intensity, the larger rate of DME production ($v = k_1\,[DME]^n$) extrapolated from the MS data for the Cu@MOR sample with respect Cu@FER and Cu@ZSM-5 could also be related to the enhanced production of DME attained within 12-MR channels. The analysis of the MS data also revealed opposite tendencies with similar slopes for the DME formation and CO–Cu^+ species disappearance (dashed line extrapolated from 2156 cm^{-1} band evolution). Thus, as the CO–Cu^+ disappeared, increments of the band ascribed to the CO–Cu-DME (2132 cm^{-1}) suggesting that a reaction intermediate is being formed. Thus, it could be argued that the rate of DME formation relates to the insertion of CO molecules into CO–Cu^+ sites which result in methyl acetate species. The observed trends remark the relevance of employing bifunctional systems in which, either Brønsted acid or Cu redox sites, play fundamental roles for the DME production. Concerning acetic acid formation, it is plausible to propose that it occurs through the insertion of another CO molecule into CO–Cu-DME (2132 cm^{-1}). This subsequent insertion results in the regeneration of methoxy species and methyl acetate (m/z = 74) species. The acetic acid (m/z = 60) might be constituted through the hydration of methoxy species or through the hydrolysis of regenerated methoxides [29].

3.5. Mechanistic considerations

According to the obtained outcomes, the reaction pathway for the carbonylation of methanol should involve the following steps: i) Adsorption and dehydration of methanol in the Brønsted acid sites inside the zeolite cavities resulting in the constitution of methoxy and dimethyl ether species. ii) Adsorption of CO over the Cu^+ metal sites generating a CO–Cu^+ which react with DME to constitute a CO-(Cu)-DME intermediate; and iii) the CO-(Cu)-DME intermediate migrates and, through a subsequent CO insertion, generates a methyl acetate intermediate which via hydrolysis produce acetic acid. The methoxy group might form acetic acid via a subsequent hydration process. The proposed reaction pathway, sketched in Fig. 8, partially agrees with the reaction mechanisms previously suggested [5,29] with the major difference relaying on the role Cu species. These works suggest that Cu carbonyl species do not participate in the reaction and relates the major role of Cu species to the DME stabilization suppressing the hydrocarbon formation. In agreement with previous works [8], the simultaneous Cu^+-CO band decrease and DME-(Cu)–CO band increase coupled to the parallel DME evolution points the Cu carbonyl species as major players for the methanol

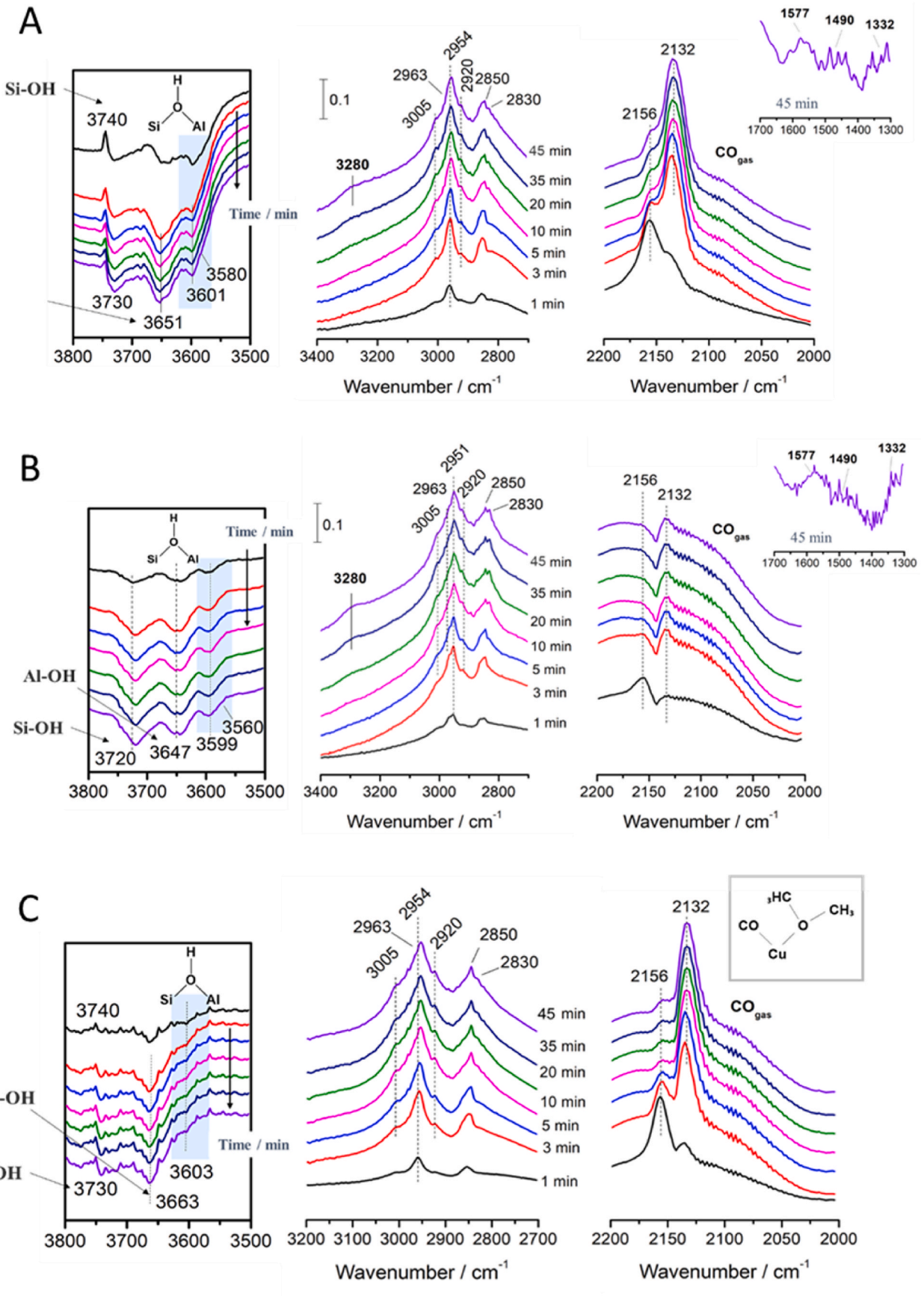

Fig. 6. *Operando* DRIFTS spectra obtained at 200 °C and 1 bar under methanol carbonylation atmospheres: A) Cu@MOR; B) Cu@FER; and C) Cu@ZSM-5.

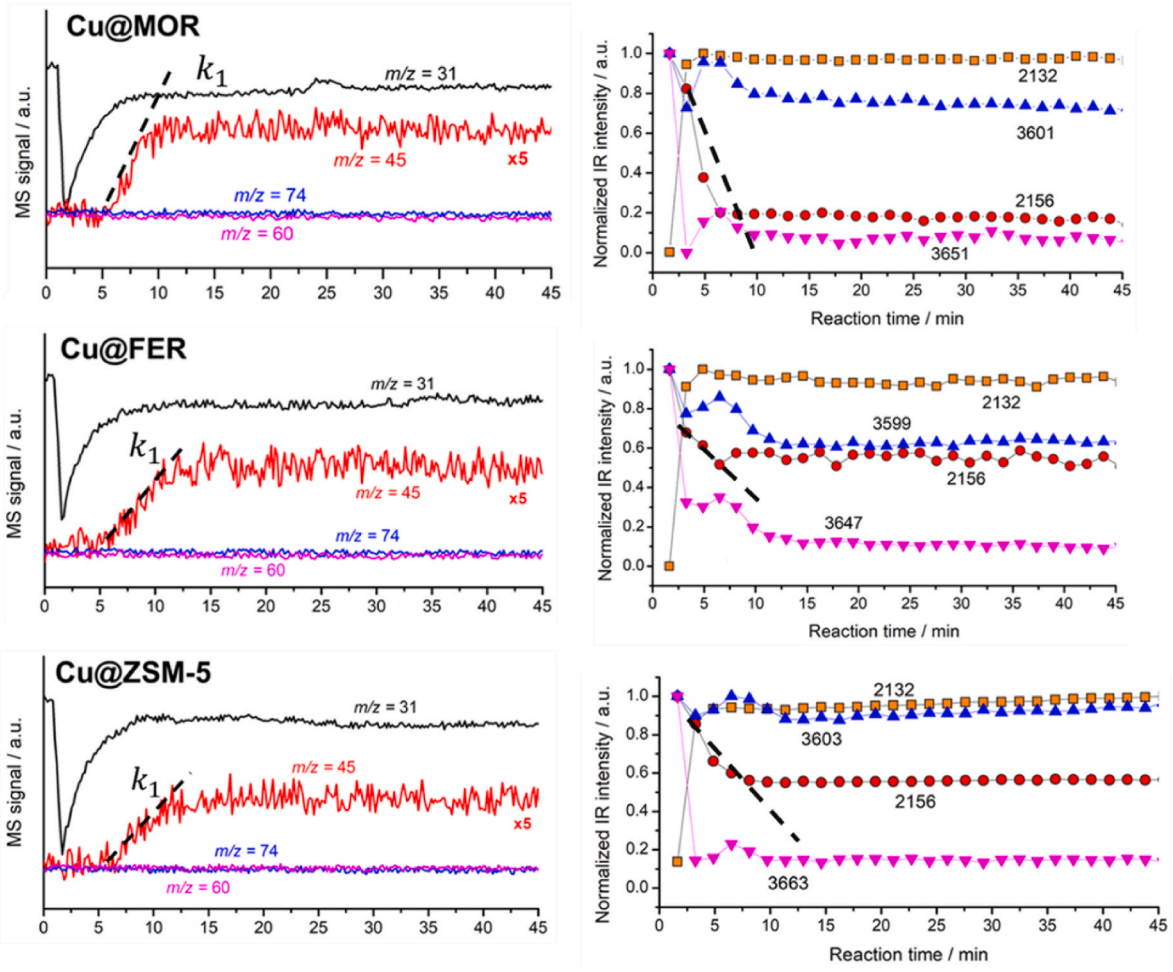

Fig. 7. Evolution of the reactant and surface intermediate bands followed by mass spectroscopy (left) and reaction intermediates adsorbed in the catalysts surface (right).

carbonylation through the activation and stabilization of carbonyl species.

4. Conclusions

This work has systematically investigated the performance of Cu-exchanged zeolites with different topology for the methanol carbonylation reaction via *operando* DRIFTS-MS. Overall, this study reaches 60% of conversion and high selectivity to the desired products for the methanol carbonylation process using economical Cu-based zeolitic solids as heterogeneous catalysts. The comparable acidity and textural properties exhibited by the systems enabled establishing a methanol carbonylation reaction pathway based on reaction intermediates developed over the catalysts' surface. The improved catalytic methanol conversions reached by Cu@FER, compared to Cu@MOR and Cu@ZSM-5, was ascribed to the larger concentrations of Brønsted acids contained within FER structures. Remarkable differences with respect to the process selectivity were discerned among the studied zeolites. In this sense, the importance of 8-MR lateral pockets is identified as vital sites for the generation of acetic acid via methanol carbonylation. In agreement, the Cu@ZSM-5 exhibited complete selectivity to DME with no observable production of acetic acid. Furthermore, the larger acetic acid and methyl acetate production attained by Cu@MOR (12-MR) and Cu@FER (10-MR) was ascribed to the constituting 12-MR and 10-MR channels, respectively. The highest rate of DME formation displayed by Cu@MOR also demonstrated the leading role played by 12-MR channels for this type of reaction.

Operando DRIFTS-MS results suggest that methanol dehydration takes place over the Brønsted acid sites located inside 8-MR channels, producing methoxy and dimethyl ether intermediates. Afterward, these react with the CO molecules activated over Cu^+ sites, generating a reaction intermediate which, through a subsequent CO insertion, generates a methyl acetate intermediate. Within the proposed dual-site mechanism, Cu^+ role is associated to the activation and stabilization of carbonyl species.

CRediT authorship contribution statement

L.A. Luque-Álvarez: Writing – original draft, Visualization, Methodology, Investigation, Data curation, Conceptualization. **M. Serrano-Cruz:** Visualization, Investigation. **M. González-Castaño:** Writing – review & editing, Writing – original draft, Validation, Data curation. **L.F. Bobadilla:** Writing – review & editing, Validation, Supervision, Methodology, Conceptualization. **J.A. Odriozola:** Supervision, Funding acquisition.

Declaration of competing interest

The authors declare that they have no known competing financial interests or personal relationships that could have appeared to influence the work reported in this paper.

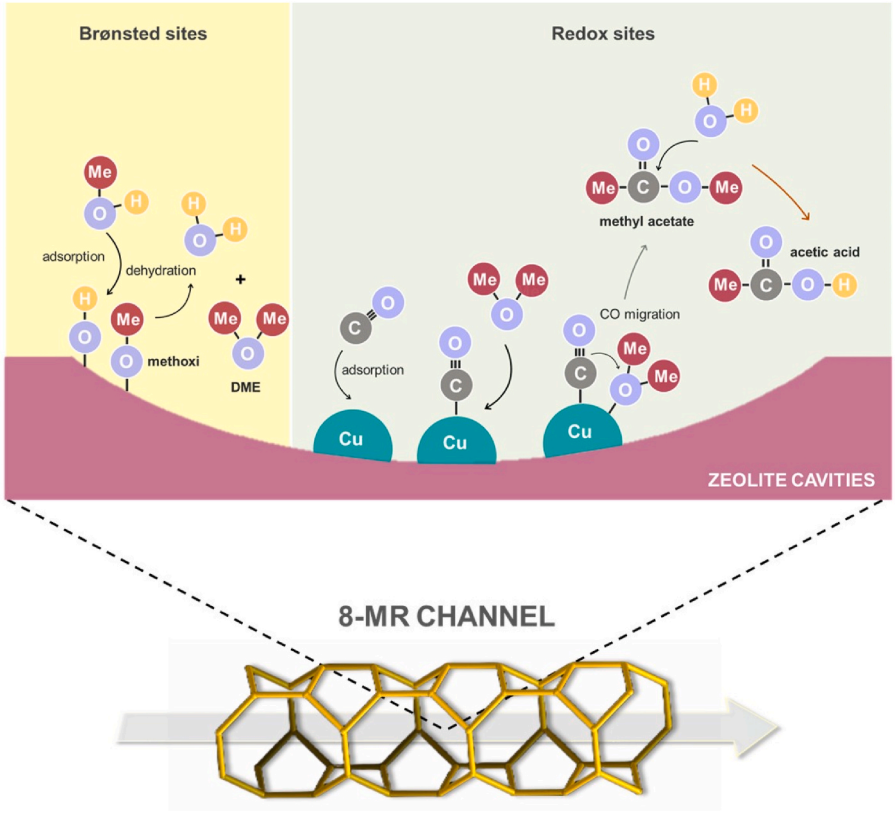

Fig. 8. Suggested reaction pathway for methanol carbonylation over Cu-zeolites.

Data availability

No data was used for the research described in the article.

Acknowledgements

Financial support for this work has been obtained from the Spanish Ministerio de Ciencia e Innovación through the project SMART-FTS (PID2021-126876OB-I00). Miriam González Castaño acknowledges the University of Sevilla for her postdoctoral contract Maria Zambrano (MZAMBRANO-2021-198). Ligia A. Luque Álvarez thanks VI-PPITUS (University of Sevilla) for her current predoctoral contract. Moreover, Melania Serrano Cruz thanks the SECAT (Sociedad Española de Catálisis) for the grant of a scholarship to carry out the master's thesis.

Appendix A. Supplementary data

Supplementary data to this article can be found online at https://doi.org/10.1016/j.micromeso.2023.112725.

References

[1] Wiese Klaus-Diether, D. Obst, Hydroformylation, Catalytic Carbonylation Reactions., 2006.
[2] P. Kalck, C. Le Berre, P. Serp, Recent advances in the methanol carbonylation reaction into acetic acid, Coord. Chem. Rev. 402 (2020), 213078, https://doi.org/10.1016/j.ccr.2019.213078.
[3] A. Haynes, Catalytic Methanol Carbonylation, first ed., Elsevier Inc., 2010 https://doi.org/10.1016/S0360-0564(10)53001-3.
[4] G.J. Sunley, D.J. Watson, High productivity methanol carbonylation catalysis using iridium. The CativaTM process for the manufacture of acetic acid, Catal. Today 58 (2000) 293–307, https://doi.org/10.1016/S0920-5861(00)00263-7.
[5] L. Zhou, S. Li, G. Qi, Y. Su, J. Li, A. Zheng, X. Yi, Q. Wang, F. Deng, Methanol carbonylation over copper-modified mordenite zeolite: a solid-state NMR study, Solid State Nucl. Magn. Reson. 80 (2016) 1–6, https://doi.org/10.1016/j.ssnmr.2016.10.003.
[6] M. Boronat, C. Martínez, A. Corma, Mechanistic differences between methanol and dimethyl ether carbonylation in side pockets and large channels of mordenite, Phys. Chem. Chem. Phys. 13 (2011) 2603, https://doi.org/10.1039/c0cp01996h.
[7] K. Fujimoto, T. Shikada, K. Omata, H. Tominaga, Vapor phase carbonylation of methanol with solid acid catalysts, Chem. Lett. (1984) 2047–2050.
[8] X. Meng, H. Guo, Q. Wang, Y. Xiao, C. Chen, B. Hou, D. Li, Elucidating the nature and role of copper species in catalytic carbonylation of methanol to methyl acetate over copper/titania-silica mixed oxides, Catal. Sci. Technol. 7 (2017) 3511–3523, https://doi.org/10.1039/c7cy00719a.
[9] T. He, P. Ren, X. Liu, S. Xu, X. Han, X. Bao, Direct observation of DME carbonylation in the different channels of H-MOR zeolite by continuous-flow solid-state NMR spectroscopy, Chem. Commun. 51 (2015) 16868–16870, https://doi.org/10.1039/c5cc07201h.
[10] T. He, X. Liu, S. Xu, X. Han, X. Pan, G. Hou, X. Bao, Role of 12-ring channels of mordenite in DME carbonylation investigated by solid-state NMR, J. Phys. Chem. C 120 (2016) 22526–22531, https://doi.org/10.1021/acs.jpcc.6b07958.
[11] X. Huang, M. Ma, M. Li, W. Shen, Regulating the location of framework aluminium in mordenite for the carbonylation of dimethyl ether, Catal. Sci. Technol. 10 (2020) 7280–7290, https://doi.org/10.1039/d0cy01362e.
[12] T. Xu, H. Liu, Q. Zhao, S. Cen, L. Du, Q. Tang, Conversion of chloromethane to propylene over fluoride-treated H-ZSM-35 zeolite catalysts, Catal. Commun. 119 (2019) 96–100, https://doi.org/10.1016/j.catcom.2018.10.029.
[13] D. Yao, H. Yang, H. Chen, P.T. Williams, Investigation of nickel-impregnated zeolite catalysts for hydrogen/syngas production from the catalytic reforming of waste polyethylene, Appl. Catal. B Environ. 227 (2018) 477–487, https://doi.org/10.1016/j.apcatb.2018.01.050.
[14] A. Smuszkiewicz, P.D.E. Doctorado, E.N. Ciencias, Tesis Doctoral Año 2017 Sílices Mesoporosas Como Nanocatalizadores, 2017.
[15] G. Leofanti, M. Padovan, G. Tozzola, B. Venturelli, Surface area and pore texture of catalysts, Catal. Today 41 (1998) 207–219, https://doi.org/10.1016/S0920-5861(98)00050-9.
[16] J. Ahmadpour, M. Taghizadeh, Selective production of propylene from methanol over high-silica mesoporous ZSM-5 zeolites treated with NaOH and NaOH/tetrapropylammonium hydroxide, Compt. Rendus Chem. 18 (2015) 834–847, https://doi.org/10.1016/j.crci.2015.05.002.
[17] W. Liu, Y. Wang, C. Sun, J. Lu, S. Wu, M. Shi, L. Bu, Z. Wang, Y. Zhi, M. Yang, Preparation of shaped binderless mordenite catalysts with controllable crystal sizes and their carbonylation performance, Mater. Chem. Phys. 292 (2022), 126823, https://doi.org/10.1016/j.matchemphys.2022.126823.
[18] K. Leistner, K. Xie, A. Kumar, K. Kamasamudram, L. Olsson, Ammonia desorption peaks can Be assigned to different copper sites in Cu/SSZ-13, Catal. Lett. 147 (2017) 1882–1890, https://doi.org/10.1007/S10562-017-2083-8/TABLES/4.
[19] S.S.R. Putluru, L. Schill, A.D. Jensen, R.S.N. Fehrmann, Selective catalytic reduction of NO_x with NH_3 on Cu-, Fe-, and Mn-zeolites prepared by impregnation:

comparison of activity and hydrothermal stability, J. Chem. 2018 (2018), 8614747, https://doi.org/10.1155/2018/8614747.
[20] R. Poreddy, S. Mossin, A.D. Jensen, A. Riisager, Promoting effect of copper loading and mesoporosity on Cu-MOR in the carbonylation of dimethyl ether to methyl acetate, Catalysts 11 (2021), https://doi.org/10.3390/catal11060696.
[21] A.K.S. Clemens, A. Shishkin, P.A. Carlsson, M. Skoglundh, F.J. Martínez-Casado, Z. Matej, O. Balmes, H. Härelind, Reaction-driven ion exchange of copper into zeolite SSZ-13, ACS Catal. 5 (2015) 6209–6218, https://doi.org/10.1021/acscatal.5b01200.
[22] C. Paolucci, J.R. Di Iorio, W.F. Schneider, R. Gounder, Solvation and mobilization of copper active sites in zeolites by ammonia: consequences for the catalytic reduction of nitrogen oxides, Acc. Chem. Res. 53 (2020) 1881–1892, https://doi.org/10.1021/acs.accounts.0c00328.
[23] E. Zhan, Z. Xiong, W. Shen, Dimethyl ether carbonylation over zeolites, J. Energy Chem. 36 (2019) 51–63, https://doi.org/10.1016/j.jechem.2019.04.015.
[24] M. Lusardi, T.T. Chen, M. Kale, J.H. Kang, M. Neurock, M.E. Davis, Carbonylation of dimethyl ether to methyl acetate over SSZ-13, ACS Catal. 10 (2020) 842–851, https://doi.org/10.1021/acscatal.9b04307.
[25] M. Boronat, C. Martínez-Sánchez, D. Law, A. Corma, Enzyme-like specificity in zeolites: a unique site position in mordenite for selective carbonylation of methanol and dimethyl ether with CO, J. Am. Chem. Soc. 130 (2008) 16316–16323, https://doi.org/10.1021/ja805607m.
[26] S. Bordiga, C. Lamberti, F. Geobaldo, A. Zecchina, G.T. Palomino, C.O. Areán, Fourier-transform infrared study of CO adsorbed at 77 K on H-mordenite and alkali-metal-exchanged mordenites, Langmuir 11 (1995) 527–533, https://doi.org/10.1021/la00002a027.
[27] N.S. Nesterenko, F. Thibault-Starzyk, V. Montouillout, V.V. Yuschenko, C. Fernandez, J.P. Gilson, F. Fajula, I.I. Ivanova, Accessibility of the acid sites in dealuminated small-port mordenites studied by FTIR of co-adsorbed alkylpyridines and CO, Microporous Mesoporous Mater. 71 (2004) 157–166, https://doi.org/10.1016/j.micromeso.2004.03.028.
[28] K. Hadjiivanov, H. Knözinger, FTIR study of low-temperature CO adsorption on Cu-ZSM-5: evidence of the formation of $Cu^{2+}(CO)_2$ species, J. Catal. 191 (2000) 480–485, https://doi.org/10.1006/jcat.1999.2805.
[29] T. Blasco, M. Boronat, P. Concepción, A. Corma, D. Law, J.A. Vidal-Moya, Carbonylation of methanol on metal-acid zeolites: evidence for a mechanism involving a multisite active center, Angew. Chem., Int. Ed. 46 (2007) 3938–3941, https://doi.org/10.1002/anie.200700029.